

Theoretical Investigation of Li and Na Oxides Adsorption on TiC(111) Surface for Metal-Air Rechargeable Batteries

Keren Raz,^{1,*} Polina Tereshchuk,^{2,*} Diana Golodnitsky,¹ and Amir Natan^{2,3,†}

¹*School of Chemistry, Tel Aviv University, Israel*

²*Department of Physical Electronics, Tel Aviv University, Israel 69978*

³*The Sackler Center for Computational Molecular and Materials Science, Tel-Aviv University, Tel-Aviv 69978, Israel*

(Dated: January 20, 2022)

We analyze, with Density Functional Theory (DFT) calculations, the adsorption energies of Li_2O_2 , Na_2O_2 and NaO_2 on clean and oxygen passivated TiC (111) surfaces. We show, that after deposition of two molecular layers of alkali metal oxides, the initial state of the TiC surface becomes unimportant for the adsorption energy and that all adsorption energies approach their native crystal values. The structure of the adsorbed molecular layers is analyzed and compared to their native oxide crystal structure. Finally, we discuss the possible implications for electrode optimization for Li-air and Na-air batteries.

I. INTRODUCTION

Rechargeable metal-air batteries are widely considered to be the next generation high-energy-density electrochemical storage devices. The intense interest in Li-air and Na-air batteries stems from their high theoretical specific energy, which exceeds that of lithium-ion batteries [1–11]. The high specific energy densities of metal-air batteries result from the use of alkali metals as anodes and ambient-air oxygen, as cathode materials. The discharge process in Li-air batteries involves an electrochemical reaction between Li^+ ions and O_2 to form Li_2O_2 onto the cathode surface. During charging, oxidation of lithium peroxide, followed by generation of oxygen gas occurs.

The optimization of charge and discharge processes involves careful design of the cathode material, the electrolytes, solvents, and mediators. The selection of solvents may affect whether the discharge products are formed at the cathode surface, or in the solution, and the prevalence of un-wanted side reactions [11, 12].

The performance and rechargeability of metal-air cells strongly depends on the positive electrode material, where oxygen reduction and evolution reactions take place. A suitable cathode material for an aprotic alkali metal/air cell should have sufficient electronic conductivity, low density, high stability over the operating voltage of the cathode towards nucleophilic attack by LiO_2 and O_2^{2-} , low cost, and non-toxicity [11]. Carbon has been the material of choice for the porous cathode. It is known that carbon oxidizes above 4V versus Li. However, more importantly, carbon raises problems that impede its use in Li/ O_2 cells. Carbon decomposes during oxidation of Li_2O_2 on charging above 3V as a result of the attack by intermediates of Li_2O_2 oxidation and it actively promotes electrolyte decomposition on discharge and charge, rendering it unsuitable for aprotic Li/ O_2 cells [13, 14].

Titanium carbide can overcome some of the disadvantages of carbon [14]. Recently, nanocrystalline TiC has been shown to be an efficient gas diffusion cathode [14]. TiC has good metallic conductivity. Furthermore, the

formation of a passivating *monolayer* of TiO_2 on the TiC surface was reported to be vital to the system's cycleability. The atomic oxide layer greatly reduces side reactions associated with electrode and electrolyte degradation at the electrolyte/cathode interface as compared with carbon [14–16].

While the Li-air battery has the highest theoretical energy density [8–11, 17], the low availability of lithium might lead to future depletion. In contrast to lithium, there are abundant sodium sources in both the earth's crust (2.3%) and in the oceans (1.1%) [18]. Moreover, the production of sodium is cheaper than that of lithium. Na-air battery systems have a lower theoretical specific energy density compared to Li-air battery systems (1605 or 1108 Wh kg⁻¹ considering Na_2O_2 or NaO_2 as discharge products, respectively). However, Na-air batteries also demonstrate lower charge/discharge overpotential, which may result in better durability [3]. Therefore, Na- O_2 battery offers an interesting alternative to the Li- O_2 battery. Even though sodium and lithium share many physicochemical properties, the chemistry of the Li-air and Na-air cells is not the same. While sodium forms stable sodium superoxide, lithium superoxide is thermodynamically unstable [18]. It is expected that both sodium peroxide and superoxide would be formed under different physicochemical conditions, however kinetic factors, temperature and oxygen pressure, the type of support and catalysts may stabilize a certain phase over the other [19, 20].

A key process of lithium-air and sodium-air systems is the possible adsorption of reaction products and intermediates at the cathode surface. The surface adsorption energy and product growth (e.g., Na_2O_2) at the surface, can be compared to the energetics of product formation in solution, where both kinetics and Li^+ and Na^+ energetics can affect the final result. Recently, the adsorption of Li_2O_2 clusters on the TiC(111) surface was theoretically investigated by Wang et al. [21, 22] using density functional theory.

In this work we performed ab-initio DFT simulations of $n\text{Li}_2\text{O}_2$, $n\text{Na}_2\text{O}_2$ and $n\text{NaO}_2$ ($n = 1–6$) molecular ad-

sorption on the pristine and oxidized TiC(111) surfaces. We investigated structural and adsorption energy trends as a function of molecular density on both pristine and oxygen passivated TiC(111) surfaces. The highest magnitude of the adsorption energy was found for molecules on the pristine surface at $n = 1, 2$ that bind directly with the reactive Ti-terminated surface, forming O–Li/Na bilayers. At larger molecular density of alkali metal oxides (AMO) there is a reduction in adsorption energy and finally after two molecular layers of AMO the adsorption energy gain reaches an almost constant value close to the AMO native crystal growth energy because of no direct contact with the TiC surface. We also discuss the work function and d-band shift as a function of AMO surface density. Finally, we discuss the possible implications of our results for the optimization of TiC and other electrode materials for Li-air and Na-air batteries.

II. THEORETICAL APPROACH AND COMPUTATIONAL DETAILS

For the total energy calculations we have used Density Functional Theory (DFT) with the generalized gradient approximation (GGA) [23] functional as proposed by Perdew, Burke, and Ernzerhof (PBE) [24]. Since titanium is a transition metal, one might consider utilization of the Hubbard correction (PBE+ U). In addition, Van der Waals (VdW) corrections might affect the adsorption properties of the systems considered. We analyze both effects in the supporting information (SI) and show that they do not significantly change our conclusions. We therefore use the PBE functional throughout all the calculations that are shown here.

To solve Kohn-Sham DFT equations we used projected augmented wave (PAW) pseudopotentials [25, 26] as implemented in the Vienna Ab-initio Simulations Package (VASP) [27, 28]. We used a Monkhorst-Pack \mathbf{k} -point sampling scheme [29] with \mathbf{k} -point meshes of $11 \times 11 \times 11$, $11 \times 11 \times 1$ and gamma point for the bulk, surface and gas-phase molecules, respectively, and a cutoff energy of 500 eV for all the calculations, except for the bulk calculations, in which a higher cutoff was used for the stress tensor minimization procedure. The structures were considered as optimized to their ground state geometries when the atomic forces per atom were smaller than 0.02 eV per Å and a total energy convergence of 10^{-6} eV was achieved.

To model the TiC, Li_2O_2 and Na_2O_2 bulks and surfaces we used the AFLOW [30] package and the ICSD database [31]. The TiC(111) surface was constructed by applying the repeated slab model with 8 layers, 2×2 surface unit cell and 21 Å vacuum region, which was found to be sufficient. Thicker slabs of TiC were shown to give similar results and are discussed in the SI. We found that the Ti-terminated TiC(111) surface is more stable than the C-terminated TiC(111) surface, which is supported by previous results [21, 32, 33]. Thus, for our fur-

ther simulations of the molecules on TiC(111) we use the Ti-terminated TiC(111) surface. The oxidized TiC(111) surface was modelled by covering the Ti-terminated TiC(111) surface by oxygen atoms at the positions of the next imaginary layer of carbon atoms layer. Our calculated surface energy for the Ti-terminated TiC(111) surface, 201.8 meV/Å², is slightly lower than the result reported by Wang *et. al.* (208 meV/Å²) [21].

A. Atomic structure generation of $n\text{M}_2\text{O}_2$ ($\text{M} = \text{Li, Na}$) and $n\text{MO}_2$ ($\text{M} = \text{Na}$) ($n = 1-6$) on TiC(111) surface

The adsorption geometry of the AMOs is first dictated by the reactive TiC surface. As more AMO layers are formed, the geometry becomes less affected by the TiC surface and should eventually approach that of the native AMO crystal. Hence, the resulting geometry of the first layers is somewhere in between the positions dictated by the TiC surface and the AMO native crystal. This gradual change makes the finding of a global minimum for the geometry a greater challenge. We simulated, as an initial guess, different $n\text{Li}_2\text{O}_2$, $n\text{Na}_2\text{O}_2$, and $n\text{NaO}_2$ ($n = 1-6$) structures on the pristine and oxidized TiC(111) surfaces by applying the following procedures which are described below in the text: (i) first-principles molecular dynamics (MD) simulations, (ii) finding a common crystalline cell and (iii) cross-check procedure. In all of the calculations we placed the molecules on one side of the slab and employed dipole correction in order to obtain accurate total energies. We allowed the molecules to relax along with four slab layers, while the remaining bottom layers were frozen.

The details of the simulations are as follows:

(i) **MD simulations:** we performed MD simulations by applying the Nosé thermostat and slowly lowering the temperature from 300 K (and 500 K) to 0 K for 30 ps. The initial structural models were built by putting the optimized gas-phase Li_2O_2 , Na_2O_2 and NaO_2 molecules at random positions at about 3 – 4 Å above the pristine and oxidized TiC(111) surfaces.

(ii) **Common crystalline cell:** In order to investigate the crystal Li_2O_2 , Na_2O_2 , and NaO_2 structures on the TiC(111) surfaces we employed the geometrical lattice match algorithm proposed by Zur and McGill [34]. This algorithm can be successfully used to fit superlattices with any pair of crystals and surfaces. Thus, we created a common cell for the hexagonal $\text{Li}_2\text{O}_2(001)$ and $\text{Na}_2\text{O}_2(001)$ surfaces on the hexagonal TiC(111) surface, and cubic $\text{NaO}_2(001)$ surface on the hexagonal TiC(111) surface.

It can be shown that $2\text{Li}_2\text{O}_2(001)$ and $2\text{NaO}_2(001)$ form a full layer at the (2×2) TiC(111) surface hexagonal unit cell, and so we built the crystal structures with $n = 2, 4$ and 6 , which represent one, two and three crystal layers, respectively. For the case of $\text{Na}_2\text{O}_2(001)$ crystal, a full monolayer coverage occurs at $n = 1.5$, which

implies the coverage of 2 and 4 crystal layers at $n = 3$ and 6, respectively. This happens because although the (2×2) TiC(111) surface unit cell is commensurate with the Na_2O_2 crystal, it cannot accommodate an integer number of molecules for a single and full molecular layer of its native crystal. In order to achieve complete crystal layer coverage by an integer number of molecules, we repeated our calculations with a larger rectangular surface cell that has twice the surface area. The results of these calculations can be found in SI and generally agree with the analysis of the smaller cell.

(iii) **Cross-check procedure:** Finally, we performed cross-check between the lowest energy structures of $n\text{Li}_2\text{O}_2$ and $n\text{Na}_2\text{O}_2$ with the aim of investigating additional possible configurations. We took the lowest energy $n\text{Li}_2\text{O}_2$ structure and used it as a starting point for geometrical relaxation of the respective $n\text{Na}_2\text{O}_2$ system, and vice-versa. This was helpful in some particular cases to find lower energy structures that were missed by the MD procedure.

Thus, we constructed about 4-5 initial configurations for every system, which were finally optimized with the standard optimization procedure applying the conjugated gradient algorithm as implemented in VASP. Finally, we collected all these structures and selected the lowest energy configurations, which were used for further analyses.

III. RESULTS

A. TiC, Li_2O_2 , Na_2O_2 and NaO_2 bulks, common cells and gas-phase molecules

Titanium carbide (TiC) bulk has a face centered cubic (fcc) structure with the O_h^5 space group symmetry. Our calculated TiC equilibrium lattice constant, $a = 4.337$ Å, is close to the thermal expansion experimental value (4.318 Å) [35] and recent PBE calculations (4.333 Å) [22]. Li_2O_2 and Na_2O_2 bulks crystallize in hexagonal $P6_3/mmc$ and $P6_2m$ space groups, respectively. The lattice parameters we obtained are 3.158 Å and 7.686 Å for Li_2O_2 and 6.195 Å and 4.472 Å for Na_2O_2 , in good agreement with the experimental values [36] and previous theoretical GGA results [22, 37, 38]. NaO_2 can crystallize in a pyrite structure in $Pa3$ space group (between 196 and 223 K), and in $Fm3m$ space group (above 223 K), which corresponds to a pyrite structure with a disorder of O_2 orientation, as obtained by powder and single crystal X-ray diffraction methods [39]. Our calculated structure corresponds to the ordered pyrite structure in $Pa3$ space group with a calculated lattice parameter of 5.521 Å, which is in a good agreement with other PBE calculations (5.509 Å) [40] and experiment [39]. The lattice parameters calculated by us along with the corresponding literature values can be found in the SI.

For the common cells created, $\text{Li}_2\text{O}_2(001)/\text{TiC}(111)$, $\text{Na}_2\text{O}_2(001)/\text{TiC}(111)$ and $\text{NaO}_2(001)/\text{TiC}(111)$, we cal-

culated a misfit factor $\eta = (1 - \frac{2\Omega}{\Omega+A}) \cdot 100\%$, as defined by Wang *et al.* [22], and an area ratio $\alpha = \frac{A}{\Omega}$, where Ω is the surface area of TiC(111) (32.597 Å²) and A is the original surface area of $\text{Li}_2\text{O}_2(001)$ (34.543 Å²), $\text{Na}_2\text{O}_2(001)$ (33.237 Å²) and $\text{NaO}_2(001)$ (30.484 Å²). We found a compression and a relatively small η of 2.90% and 0.97% and α of 1.06 and 1.02 for the $\text{Li}_2\text{O}_2(001)/\text{TiC}(111)$ and $\text{Na}_2\text{O}_2(001)/\text{TiC}(111)$, respectively, and an expansion with η of -3.35% and α of 0.94 for the $\text{NaO}_2(001)/\text{TiC}(111)$ cell.

To obtain the lowest energy structures of the molecules in the gas-phase, we selected reasonable geometries, such as linear, square, triangle and rhombus for Li_2O_2 and Na_2O_2 molecules, and linear and triangle for the NaO_2 molecule to be optimized. We found that the lowest energy structures for the Li_2O_2 and Na_2O_2 molecules are the planar rhombus, in which two O and two Li (Na) atoms are at opposite corners with Li-O (Na-O) bond lengths of 1.74 Å (2.08 Å) and O-O bond lengths of 1.59 Å (1.60 Å). This structure is in a good agreement with the results reported by Lau *et al.* [41] for the Li_2O_2 molecule. The gas-phase structure of NaO_2 corresponds to the isosceles triangle with Na-O and O-O bond lengths of 2.13 Å and 1.37 Å, respectively. A figure that shows the lowest energy geometry for the gas-phase molecules is presented in the SI.

B. Adsorption energies

We have calculated the adsorption energy per molecule as:

$$E_{ad1}^n = (E_{tot}^{n*mol/TiC} - nE_{tot}^{molecule} - E_{tot}^{TiC})/n \quad (1)$$

where n is the number of molecules in the system and $E_{tot}^{n*mol/TiC}$, $E_{tot}^{molecule}$ and E_{tot}^{TiC} correspond to the total energies of the lowest energy structures for: $n\text{M}_2\text{O}_2$ and $n\text{MO}_2$ molecules on the non-oxidized and oxidized TiC(111) slabs, a single gas-phase molecule, and the TiC slabs, respectively.

In order to evaluate the contribution of the recently adsorbed molecule, we calculated also:

$$\begin{aligned} E_{ad2}^n &= E_{tot}^{n*mol/TiC} - E_{tot}^{(n-1)*mol/TiC} - E_{tot}^{molecule} \\ &= nE_{ad1}^n - (n-1)E_{ad1}^{n-1}. \end{aligned} \quad (2)$$

Here E_{ad1}^n and E_{ad1}^{n-1} are the adsorption energies of the n and $n-1$ molecules on the TiC(111) surfaces as defined in Eq. 1 and we define $E_{ad1}^0 = 0$.

We calculated the adsorption energies of systems with $n = 1$ to $n = 6$ molecules corresponding to molecular surface densities of $\sim 0.03[1/\text{\AA}^2]$ ($3 \times 10^{14}[1/\text{cm}^2]$) to $\sim 0.18[1/\text{\AA}^2]$ ($1.8 \times 10^{15}[1/\text{cm}^2]$). Those results are shown in Figure 1, we found similar trends in the adsorption energies (E_{ad1}) of $n\text{Li}_2\text{O}_2$, $n\text{Na}_2\text{O}_2$ and $n\text{NaO}_2$

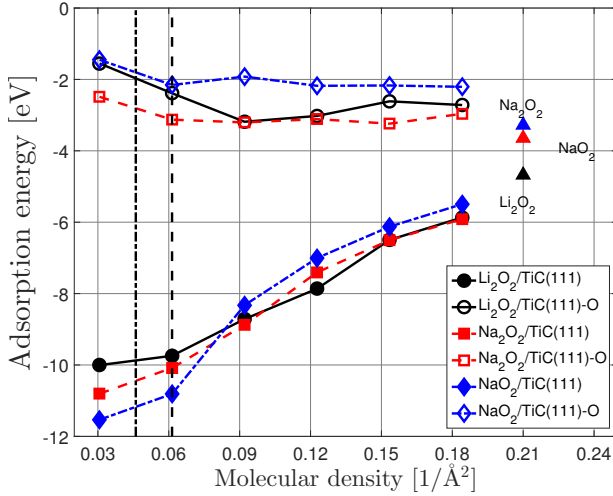


FIG. 1. The adsorption energy (Eq. 1) of $n\text{Li}_2\text{O}_2$, $n\text{Na}_2\text{O}_2$ and $n\text{NaO}_2$ molecules on TiC(111) and TiC(111)-O surfaces vs molecular density. Triangles correspond to the growth energy per molecule of the metal oxide crystals that were adapted to fit the TiC(111) surface cell. The dashed vertical lines correspond to the molecular densities that lead to a single molecular layer, i.e., 2 molecules of Li_2O_2 and NaO_2 and 1.5 molecules of Na_2O_2 in the TiC surface cell.

molecules on the TiC(111) and TiC(111)-O surfaces. For example, E_{ad1} decreases with increasing coverage of molecules on the TiC(111) surface, from -10.00 eV to -5.87 eV for 1 Li_2O_2 and 6 Li_2O_2 , respectively. This trend can be explained by the following argument: The larger value of E_{ad1} at $n=1,2$ is due to the direct binding of the molecules with the highly reactive Ti surface atoms. When increasing the number of molecules in the system, E_{ad1} tends to decrease as the additional molecules are adsorbed on top of the first molecular layer and are not in the direct contact with the TiC surface. Since the interaction between molecular layers is weaker than the interaction of the molecules with the clean and reactive TiC surface, a smaller adsorption energy is obtained.

By contrast, on the oxidized surface, the E_{ad1} of molecules follow a different trend and are in the range of -1.55 eV to -3.19 eV for $n\text{Li}_2\text{O}_2$, from -2.48 eV to -3.24 eV for $n\text{Na}_2\text{O}_2$ and -1.45 eV to -2.21 eV for $n\text{NaO}_2$ systems. This behavior shows that the oxygen layer effectively passivates the TiC surface. The AMO molecules now interact with the oxygen layer and not with the reactive Ti atoms of the pristine surface, leading to significantly lower adsorption energies for the first AMO layer. Equation 2 gives the adsorption energy of the recently added molecule; these data are shown in Figure 2. The adsorption of one and two molecules to the pristine TiC(111) surface yields more energy because of direct binding with the reactive TiC(111) surface, i.e. $E_{ad2} = -10.00$ eV for 1 Li_2O_2 , while the adsorption of the next molecules require less energy, e.g. -6.66 eV for 3 Li_2O_2 , as the molecules are above the first bilayer. Fi-

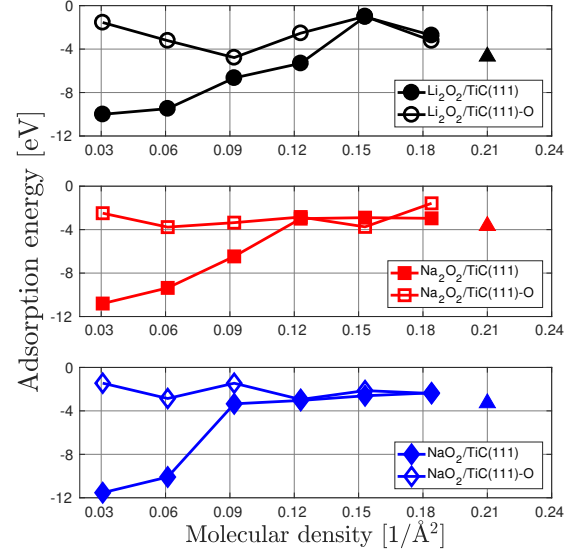


FIG. 2. The adsorption energy (Eq. 2) of Li_2O_2 , Na_2O_2 and NaO_2 on TiC(111) and TiC(111)-O surfaces per molecular density. Triangles correspond to the growth energy per molecule of the metal oxide crystals in the TiC(111) surface cell.

nally, at $n = 5$ and 6 the adsorption energy gain remains unchanged, namely, -2.73 eV for 6 Li_2O_2 , and tends to achieve the adsorption energy of the crystal structure, which is to be expected as a result of the increasing role of the intermolecular binding. Another important observation from Figure 2 is that after two molecular layers (density of 0.12 [$1/\text{\AA}^2$]), the adsorption energy for additional molecules is almost the same for the clean and oxidized surfaces for all the three AMO species.

C. Geometry of adsorbed AMO layers

We present the lowest energy structures of $n\text{M}_2\text{O}_2$ ($\text{M} = \text{Li}, \text{Na}$) and $n\text{MO}_2$ ($\text{M} = \text{Na}$) molecules on the pristine and oxidized TiC(111) surface in Figures 3, 4 and 5. In order to describe the structure of the molecules on the TiC(111) surfaces we measured the following structural parameters: the molecular surface density, ρ_{mol} , calculated as the number of molecules per surface area, the minimal Ti–O, M–O and M–M bond lengths, and the molecular layer thickness, D , calculated as the vertical distance between the M atoms nearest and farthest from the surface, which might be helpful to determine if the structure is crystal-like or distorted. All the structural parameters and the adsorption energies of the lowest energy structures are given in Table I, while the parameters of both crystal-like and distorted structures can be found in Table 3 in the SI. The structural data for the corresponding crystals and molecules is also provided in the SI for comparison.

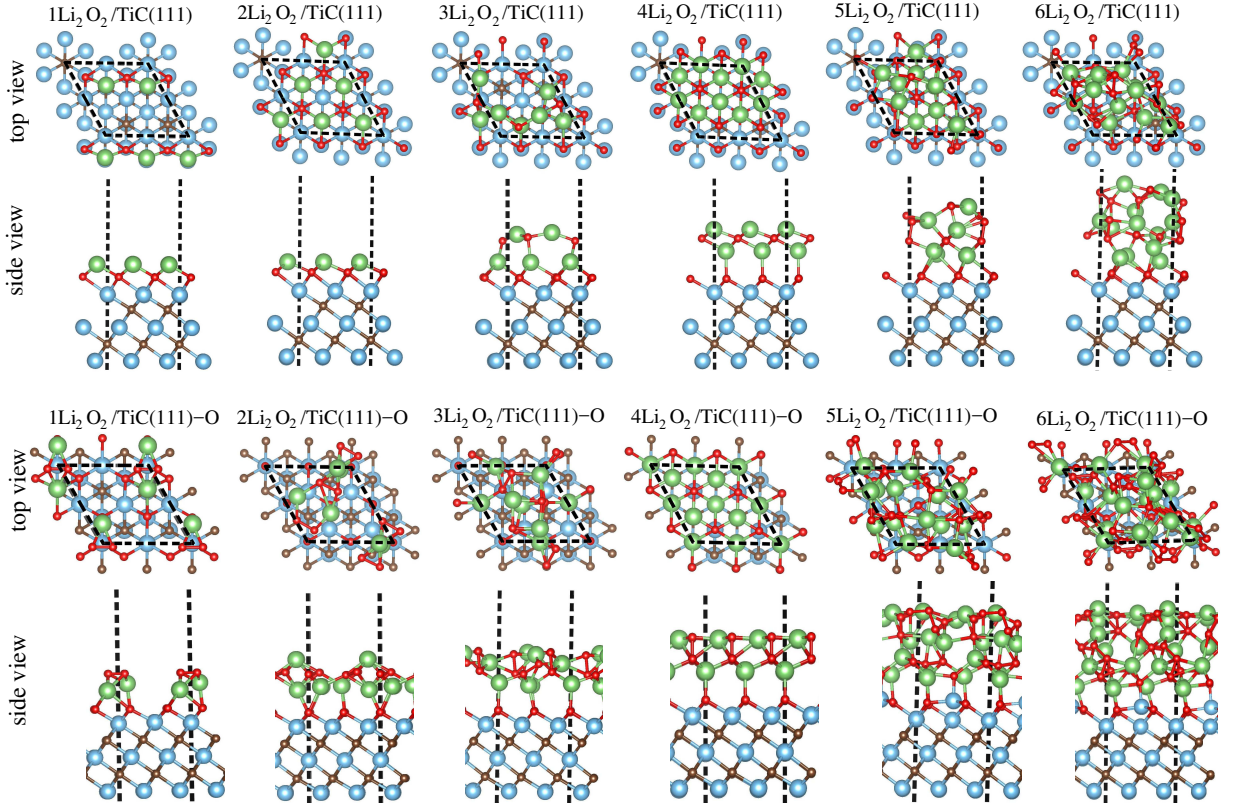


FIG. 3. Lowest energy configurations of $n\text{Li}_2\text{O}_2$ ($n = 1-4$) molecules on the non-oxidized and oxidized TiC(111). Blue and brown balls correspond to Ti and C atoms, while red and green balls are O and Li atoms, respectively. Ball sizes are drawn according to atomic radii.

The lowest energy structures of the adsorbed AMO molecules at $n = 1, 2$ (with a molecular density of ~ 0.03 [$1/\text{\AA}^2$] and 0.06 [$1/\text{\AA}^2$] respectively) on the pristine TiC(111) surface form O and M atomic layers. In this structure the O atoms are at the hcp hollow positions of Ti atoms, taking the positions of the missing C atoms. The Li/Na atoms are on fcc hollow of C atoms, on the positions of the missing Ti atoms in the next atomic layer. The M–O bond lengths are close to the corresponding crystal bonds (see Table I). The formation of the layered structures due to the creation of O–Ti bonds and the complete break of the molecular O–O bonds can be explained by the strong binding of the O atoms with the reactive Ti-terminated surface. Full molecular (2 molecules, 0.06 [$1/\text{\AA}^2$]) coverage of the TiC(111) by $2\text{M}_2\text{O}_2$ and 2MO_2 leads to the expansion of the first O layer relative to a partial coverage, for example the Ti–O bond lengths of $2\text{Li}_2\text{O}_2/\text{TiC}(111)$ increase by 0.18 \AA compared with $1\text{Li}_2\text{O}_2/\text{TiC}(111)$. Our finding is in a good agreement with the structures obtained by Wang *et. al.* [22] for $1\text{Li}_2\text{O}_2$ molecule on the TiC(111) surface.

At larger molecular density (0.09 [$1/\text{\AA}^2$] and 0.12 [$1/\text{\AA}^2$], which correspond to $n = 3$ and 4) we found that molecules resemble a layered structure arrangement with M/O/M/O molecular layers on the TiC(111) surface, in

which the lowest O atoms stay at the hcp hollow positions on the TiC(111) surface, similarly to the case of $n = 1, 2$, however, the M and O atoms of the next molecular layers are slightly displaced from their ideal atomic hcp and fcc hollow positions. The displacements are more significant for the $n\text{NaO}_2$ molecules compared with the $n\text{Li}_2\text{O}_2$ and the $n\text{Na}_2\text{O}_2$ molecules because of the different stoichiometry.

An addition of the next two molecules ($n = 5$ and 6 with the density of 0.15 [$1/\text{\AA}^2$] and 0.18 [$1/\text{\AA}^2$]) leads to large atomic displacements of the M/O/M layers, except for the first O layer bound to the TiC(111) surface. The M–O, O–O and M–M bond lengths of the distorted structures are shorter compared with the ordered structures.

To summarize this part, it is possible to say that initially the AMO atoms prefer to follow the atomic positions dictated by the TiC crystal. As more molecules are adsorbed, the structure changes in the direction of the native AMO crystal but more layers are needed to fully reach that.

The thickness, D , of the AMO molecular layers, is another parameter which can be compared with the respective D of the corresponding compressed AMO crystal structure. Figure 6 shows the layers thickness of the lowest energy structures as a function of molecular den-

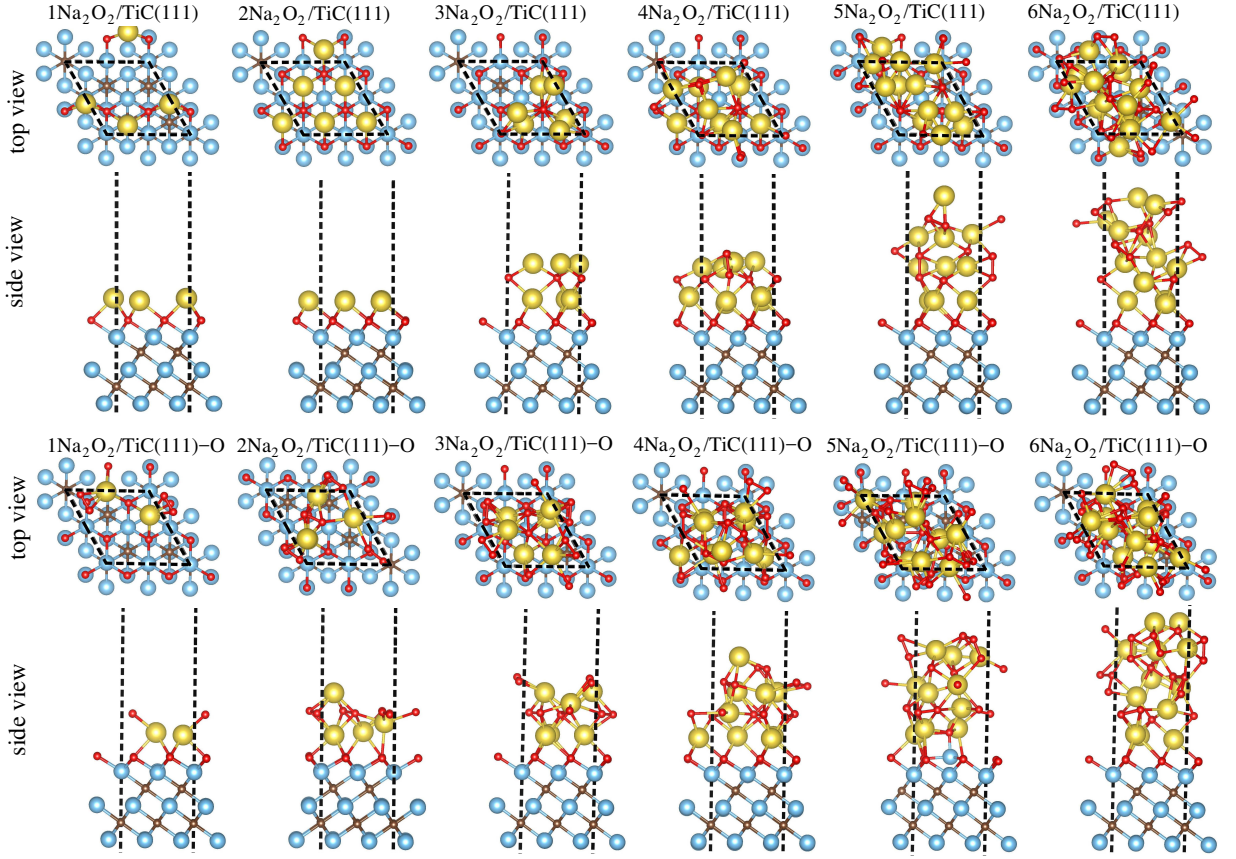


FIG. 4. Lowest energy configurations of $n\text{Na}_2\text{O}_2$ ($n = 1-4$) molecules on the non-oxidized and oxidized TiC(111). Blue, brown, red and yellow balls correspond to Ti, C, O and Na atoms, respectively. Ball sizes are drawn according to atomic radii.

sity. We found that for $n\text{Li}_2\text{O}_2$, $n\text{Na}_2\text{O}_2$, and $n\text{NaO}_2$ molecules on the pristine TiC(111) surface D is near zero at $n = 1$ and 2 showing that in the first layer all metal atoms are at about the same height, while at $n = 3$ and 4 D in most cases change only slightly with respect to the native crystal, namely by 12–19%, except for $4\text{Na}_2\text{O}_2$ and 3NaO_2 systems which change by 38% and 67%, respectively. For the larger systems (at $n = 5$ and 6) the differences in D between the adsorbed AMOs and the crystal structures are higher, for example 46% for $6\text{Li}_2\text{O}_2$.

D. The effect of surface oxidation on the geometry of the adsorbed AMO layers

The presence of an oxide layer on the TiC(111) surface, (TiC(111)-O), strongly affects the molecular structures which differ significantly from that of the pristine surface. Despite the similar trends, such as breaking molecular O–O bonds and structural reassembling, less ordered structures are already formed on the surface at $n = 1$, as a result of no direct binding with the reactive Ti atoms on the surface.

The layer thickness parameter tends to increase com-

pared with the value of D on the pristine TiC(111) surface for all systems as a result of higher structural distortions. This trend can be observed already at $n = 1$ and 2. One example is D of 0.00 Å and 2.25 Å for $2\text{Li}_2\text{O}_2$ on the pristine and oxidized TiC(111) surfaces, respectively. For higher molecular density the differences in D still exist but show an oscillating pattern.

E. d-band shift

The analysis of changes in electronic properties can reveal additional details on the effects of molecular adsorption on clean and oxygen passivated surfaces.

A shift of the center of the d band (d_s) of the surface Ti atoms after adsorption can be considered as an important parameter for the interaction of molecules with the Ti-terminated surface. On the basis of the d -band model, proposed by *Norskov et. al.* [42, 43], d_s can be used in explaining the main trends in reactivity of the transition metals, which vary with element, surface structure and alloying [44]. We present the calculated shifts, d_s , for the lowest energy systems in Figure 7. As can be expected, the shift in the center of the d states on the TiC(111) surface is larger in most cases than the

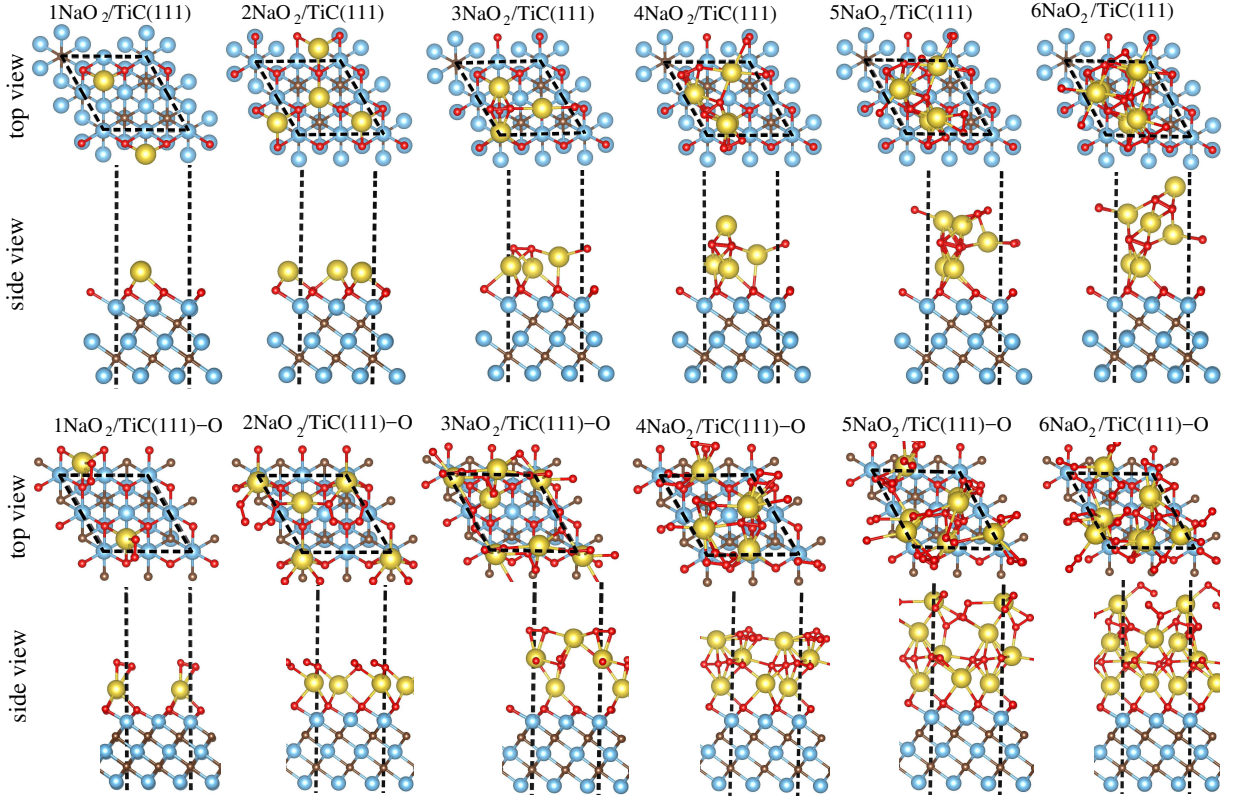


FIG. 5. Lowest energy configurations of $n\text{NaO}_2$ ($n = 1-6$) molecules on the non-oxidized and oxidized $\text{TiC}(111)$, where blue, brown, red and yellow balls present Ti, C, O and Na atoms, respectively. Ball sizes are drawn according to atomic radii.

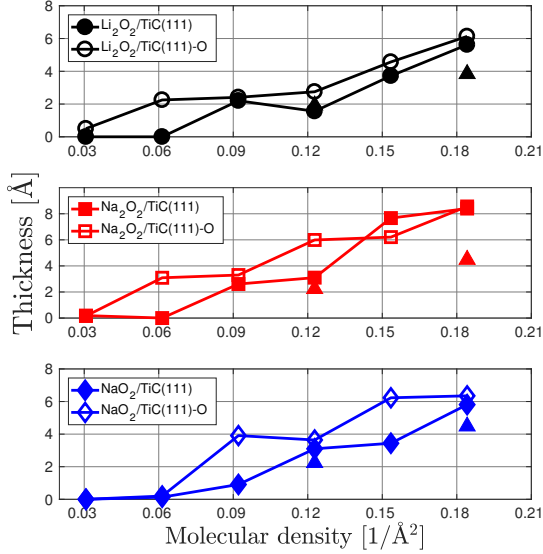


FIG. 6. The layers thickness for the lowest energy structures of $n\text{Li}_2\text{O}_2$, $n\text{Na}_2\text{O}_2$ and $n\text{NaO}_2$ molecules on $\text{TiC}(111)$ and $\text{TiC}(111)\text{-O}$ surfaces vs molecular density. Triangles up and down correspond to the thickness of the crystals in the original cell and compressed to the $\text{TiC}(111)$ cell, respectively.

shift on the $\text{TiC}(111)\text{-O}$ surface, which indicates stronger interaction of the molecules with the $\text{TiC}(111)$ surface. For example, Δd_s spreads from -1.49 eV to -3.96 eV for the $n\text{Na}_2\text{O}_2/\text{TiC}(111)$ systems, while it ranges from -0.72 eV to -2.25 eV for the $n\text{Na}_2\text{O}_2/\text{TiC}(111)\text{-O}$ systems.

Additional calculations of the local density of states (LDOS) for the lowest energy configurations are presented in the SI.

F. Work function change

Another surface property which can be calculated and measured is the change in the system work function as a function of molecular coverage. We calculated the work function (Φ) of the pristine and oxidized $\text{TiC}(111)$ surfaces before and after adsorption, and also the change in the work function of the systems, namely $-\Delta\Phi = \Phi^{n\text{M}_2\text{O}_2/\text{TiC}(111)} - \Phi^{\text{TiC}(111)}$. The work function changes are presented in Figure 8. We also show the electrostatic potentials of these systems, before and after adsorption, in the SI.

The value Φ of the pristine $\text{TiC}(111)$ surface, calculated by us, is 4.57 eV, which is close to experimental value of 4.7 eV [45]. An oxygen layer on the $\text{TiC}(111)$ results in an increase of the work function to 5.20 eV.

TABLE I. Adsorption energy, E_{ad} , and structural properties, such as minimal Ti-O, M-O and M-M bond lengths, $d_{\text{Ti-O}}^{\text{min}}$, $d_{\text{M-O}}^{\text{min}}$ and $d_{\text{M-M}}^{\text{min}}$, respectively, of the $n\text{M}_2\text{O}_2$ (M = Li, Na; $n = 1-6$) and $n\text{NaO}_2$ ($n = 1-6$) molecules with molecular density, ρ_{mol} , and thickness, D , on TiC(111) and TiC(111)-O surfaces. The data for crystal structure and molecules in gas-phase are also provided for comparison. The adsorption energies are given in eV, while the bond lengths and thickness are in Å.

n	ρ_{mol}	E_{ad}	$d_{\text{Ti-O}}^{\text{min}}$	$d_{\text{M-O}}^{\text{min}}$	$d_{\text{M-M}}^{\text{min}}$	D	E_{ad}	$d_{\text{Ti-O}}^{\text{min}}$	$d_{\text{M-O}}^{\text{min}}$	$d_{\text{M-M}}^{\text{min}}$	D
$n\text{Li}_2\text{O}_2/\text{TiC}(111)$							$n\text{Li}_2\text{O}_2/\text{TiC}(111)\text{-O}$				
1	0.031	-10.00	2.05	1.88	3.07	0.00	-1.55	2.02	1.88	2.98	0.50
2	0.061	-9.74	2.23	1.93	3.07	0.00	-2.39	2.03	1.89	2.27	2.25
3	0.092	-8.71	2.06	1.80	2.46	2.20	-3.19	2.02	1.86	2.43	2.41
4	0.123	-7.86	2.03	1.89	2.38	1.56	-3.02	2.05	1.77	2.78	2.75
5	0.153	-6.50	2.04	1.86	2.29	3.72	-2.61	2.02	1.82	2.39	4.57
6	0.184	-5.87	2.06	1.82	2.30	5.62	-2.72	2.06	1.86	2.22	6.13
crys.				1.98	2.65	1.92			1.98	2.65	1.92
mol.				1.74	3.09				1.74	3.09	
$n\text{Na}_2\text{O}_2/\text{TiC}(111)$							$n\text{Na}_2\text{O}_2/\text{TiC}(111)\text{-O}$				
1	0.031	-10.80	2.01	2.31	3.45	0.19	-2.48	2.01	2.30	3.34	0.16
2	0.061	-10.08	2.15	2.29	3.06	0.00	-3.13	2.05	2.22	3.09	3.09
3	0.092	-8.88	2.06	2.18	2.76	2.61	-3.20	2.06	2.22	2.99	3.30
4	0.123	-7.40	2.09	2.10	2.40	3.10	-3.11	2.06	2.19	2.85	5.99
5	0.153	-6.50	2.05	2.13	2.79	7.67	-3.24	1.91	2.16	2.76	6.21
6	0.184	-5.89	2.06	2.18	2.50	8.40	-2.96	2.05	2.13	2.55	8.56
crys.				2.31	3.05	2.24			2.31	3.05	2.24
mol.				2.08	3.83				2.08	3.83	
$n\text{NaO}_2/\text{TiC}(111)$							$n\text{NaO}_2/\text{TiC}(111)\text{-O}$				
1	0.031	-11.53	1.98	2.26	6.13	—	-1.45	2.00	2.35	6.13	—
2	0.061	-10.81	2.03	2.25	3.54	0.13	-2.15	2.01	2.31	3.38	0.20
3	0.092	-8.32	2.05	2.23	3.24	0.91	-1.92	2.00	2.31	3.52	3.91
4	0.123	-7.00	2.05	2.21	3.11	3.10	-2.18	2.02	2.28	3.15	3.64
5	0.153	-6.13	2.02	2.25	3.06	3.44	-2.17	2.02	2.23	3.23	6.23
6	0.184	-5.49	2.03	2.23	3.14	5.81	-2.21	2.02	2.26	3.08	6.35
crys.				2.44	3.90	2.76			2.44	3.90	2.76
mol.				2.13	—				2.13	—	

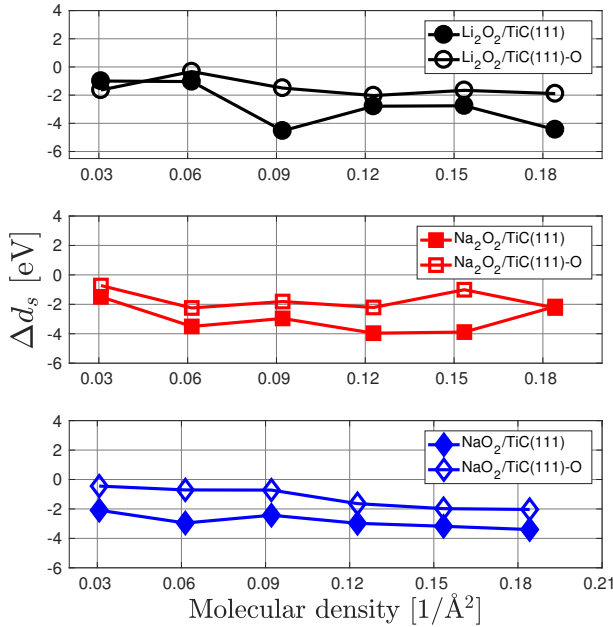


FIG. 7. The shift of the d-band center for Li_2O_2 , Na_2O_2 and NaO_2 on TiC(111) and TiC(111)-O surfaces vs molecular density per surface area.

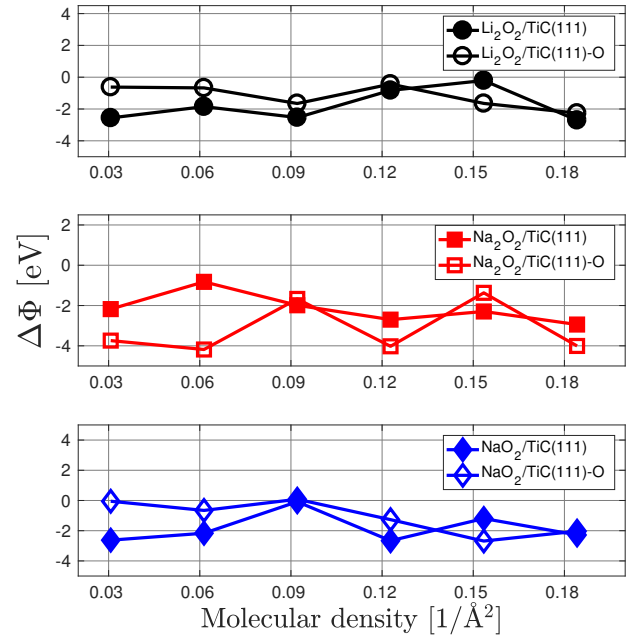


FIG. 8. The change in the work function for Li_2O_2 , Na_2O_2 and NaO_2 on TiC(111) and TiC(111)-O surfaces.

In most cases, the adsorption of the different AMO molecules leads to a reduction in the work function - $\Delta\Phi$ is negative. This can be caused either by charge transfer or polarization of the molecules on the surface or both. Examination of the changes in the work function shows that in all systems, there is no clear trend with coverage. This is to be expected as none of the grown crystals is polar and so it is logical to assume that the work function will just oscillate as more layers are grown.

IV. SUMMARY AND OUTLOOK

In this work we have calculated the adsorption energies of varying coverage of Li_2O_2 , Na_2O_2 and NaO_2 molecules on clean and oxygen passivated $\text{TiC}(111)$ surfaces. We showed that all the different AMO molecules exhibit a similar behavior and that, as would be expected, adsorption on a clean surface is initially much more favorable energetically than on an oxygen passivated surface. Furthermore, we showed that after the deposition of two molecular layers, the adsorption energies at the clean and oxygen passivated surface approach one another (see Fig. 2) and in fact the effect of the surface preparation becomes almost unimportant. This is mainly because the newly adsorbed molecules are now lying on the previous AMO molecular layers and not on the TiC itself, clean or oxygen passivated. To verify this we have compared the adsorption energies to the crystal growth energy per layer

for the respective crystals of Li_2O_2 , Na_2O_2 and NaO_2 . We see that these energies are already very close. It should be noted that for the oxygen passivated surface, which is more realistic experimentally, the adsorption energies are close to that of the crystal growth energies already from the first molecule for all the AMO species that we checked.

The molecules we have checked have the option to adsorb at the surface or to self-assemble in solution and form a cluster. Cluster formation energies are not equal to those of crystal growth and can larger at the beginning and smaller at later stages where there are different facets for the formed clusters[19]. As discussed before [12] the way Li_2O_2 is crystallized, surface adsorption vs. solution based self-assembly, is strongly affected by the solvent properties. However, the absolute surface adsorption energy may have some effect as well. It is therefore interesting to map and compare those energies for different electrode surfaces and check their possible relationship to cell performance.

ACKNOWLEDGMENTS

This work was supported by the Planning & Budgeting Committee of the Council of High Education and the Prime Minister Office of Israel, in the framework of the INREP project.

* Equal contribution author

† amirnatana@post.tau.ac.il

- ¹ E. L. Littauer and K. C. Tsai, "Corrosion of lithium in aqueous electrolyte," *J. Electrochem. Soc.* **124**, 850–855 (1997).
- ² K. M. Abraham and Z. Jiang, "A polymer electrolyte-based rechargeable lithium/oxygen battery," *J. Electrochem. Soc.* **143**, 1–5 (1996).
- ³ E. Peled, D. Golodnitsky, H. Mazor, M. Goor, and S. Avshalomov, "Parameter analysis of a practical lithium and sodium-air electric vehicle battery," *J. Power Sources* **196**, 6835–6840 (2011).
- ⁴ C. Chakkaravarthy and H. V. K. Udupa, "On the suppression of self discharge of the zinc electrodes of zinc air cells and other related battery systems," *J. Power Sources* **10**, 197–200 (1983).
- ⁵ S. Yang and H. Knickle, "Design and analysis of aluminum/air battery system for electric vehicles," *J. Power Sources* **112**, 162–173 (2002).
- ⁶ Y. Ma, N. Li, D. Li, M. Zhang, and X. Huang, "Performance of Mg-14 Li-1 Al-0.1 Ce as anode for Mg-air battery," *Journal of Power Sources* **196**, 2346–2350 (2011).
- ⁷ A. Ito, L. Zhao, S. Okada, and J. I. Yamaki, "Synthesis of nano- Fe_3O_4 -loaded tubular carbon nanofibers and their application as negative electrodes for Fe/air batteries," *J. Power Sources* **196**, 8154–8159 (2011).
- ⁸ J. Lu, L. Li, J.-B. Park, Y.-K. Sun, F. Wu, and K. Amine, "Aprotic and aqueous Li–O₂ batteries," *Chem. Rev.* **114**,

5611–5640 (2014).

- ⁹ Y. Chen, S. A. Freunberger, Z. Peng, O. Fontaine, and P. G. Bruce, "Charging a Li–O₂ battery using a redox mediator," *Nat. Chem.* **5**, 489–494 (2013).
- ¹⁰ Z. Wen, C. Shen, and Y. Lu, "Air electrode for the lithium-air batteries: Materials and structure designs," *ChemPlusChem* **80**, 270–287 (2015).
- ¹¹ P. G. Bruce, S. A. Freunberger, L. J. Hardwick, and J.-M. Tarascon, "Li–O₂ and Li–S batteries with high energy storage," *Nat. Mater.* **11**, 19 (2012).
- ¹² L. Johnson, C. Li, Z. Liu, Y. Chen, S. A. Freunberger, P. C. Ashok, B. B. Praveen, K. Dholakia, J.-M. Tarascon, and P. G. Bruce, "The role of LiO_2 solubility in O₂ reduction in aprotic solvents and its consequences for Li–O₂ batteries," *Nature chemistry* **6**, 1091–1099 (2014).
- ¹³ B. M. Gallant, "Chemical and morphological changes of LiO_2 battery electrodes upon cycling," *J. Phys. Chem. C* **116**, 20800–20805 (2012).
- ¹⁴ M. M. O. Thotiyl, S. A. Freunberger, Z. Peng, Y. Chen, Z. Liu, and P. G. Bruce, "A stable cathode for the aprotic Li–O–2 battery," *Nat. Mater.* **12**, 1050 (2013).
- ¹⁵ D. Kundu, R. Black, E. J. Berg, and L. F. Nazar, "A highly active nanostructured metallic oxide cathode for aprotic Li–O₂ batteries," *Energy Environ. Sci.* **8**, 1292–1298 (2015).
- ¹⁶ A. Y. Kozmenkova, E. Y. Kataev, A. I. Belova, M. Amati, L. Gregoratti, J. Velasco-Vélez, A. Knop-Gericke, B. Senkovsky, D. V. Vyalikh, D. M. Itkis, *et al.*, "Tuning

- surface chemistry of tic electrodes for lithium–air batteries,” *Chemistry of Materials* **28**, 8248–8255 (2016).
- 17 C.-X. Zu and H. Li, “Thermodynamic analysis on energy densities of batteries,” *Energy Environ. Sci.* **4**, 2614–2624 (2011).
 - 18 Q. Sun, Y. Yang, and Z.-W. Fu, “Electrochemical properties of room temperature sodium–air batteries with non-aqueous electrolyte,” *Electrochem. Commun.* **16**, 22–25 (2012).
 - 19 S. Kang, Y. Mo, S. P. Ong, and G. Ceder, “Nanoscale stabilization of sodium oxides: Implications for Na–O₂ batteries,” *Nano Lett.* **14**, 1016–1020 (2014).
 - 20 L. Lutz, W. Yin, A. Grimaud, D. A. D. Corte, M. Tang, L. Johnson, E. Azaceta, V. Sarou-Kanian, A. J. Naylor, S. Hamad, J. A. Anta, E. Salager, R. Tena-Zaera, P. G. Bruce, and J.-M. Tarascon, “High capacity Na–O₂ batteries: Key parameters for solution-mediated discharge,” *J. Phys. Chem. C* **120**, 20068–20076 (2016).
 - 21 Z. Wang, J. Sun, Y. Cheng, and C. Niu, “Adsorption and deposition of Li₂O₂ on TiC111 surface,” *J. Phys. Chem. Lett.* **5**, 3919–3923 (2014).
 - 22 Z. Wang, X. Chen, Y. Cheng, and C. Niu, “Adsorption and deposition of Li₂O₂ on the pristine and oxidized TiC surface by first-principles calculation,” *J. Phys. Chem. C* **119**, 25684–25695 (2015).
 - 23 J. P. Perdew, J. A. Chevary, S. H. Vosko, K. A. Jackson, M. R. Pederson, D. J. Singh, and C. Fiollhais, “Atoms, molecules, solids, and surfaces: Applications of the generalized gradient approximation for exchange and correlation pw91 reference,” *Phys. Rev. B* **46**, 6671–6687 (1992).
 - 24 J. P. Perdew, K. Burke, and M. Ernzerhof, “Generalized gradient approximation made simple,” *Phys. Rev. Lett.* **77**, 3865 (1996).
 - 25 P. Blochl, “Projector augmented-wave method,” *Phys. Rev. B* **50**, 17953–17979 (1994).
 - 26 G. Kresse and J. Joubert, “From ultrasoft pseudopotentials to the projector augmented-wave method,” *Phys. Rev. B* **59**, 1758–1775 (1999).
 - 27 G. Kresse and J. Furthmüller, “Efficient iterative schemes for ab initio total-energy calculations using a plane-wave basis set,” *Phys. Rev. B* **54**, 11169 (1996).
 - 28 J. Hafner, “Ab-initio simulations of materials using vasp: Density-functional theory and beyond,” *Journal of Computational Chemistry* **29**, 2044–2078 (2008).
 - 29 H. J. Monkhorst and J. D. Pack, “Special points for brillionin-zone integrations,” *Phys. Rev. B* **13**, 5188 (1976).
 - 30 S. Curtarolo, W. Setyawan, G. L. W. Hart, M. Jahnatek, R. V. Chepulskii, R. H. Taylor, S. Wang, J. Xue, K. Yang, O. Levy, M. J. Mehl, H. T. Stokes, D. O. Demchenko, and D. Morgan, “Aflow: An automatic framework for high-throughput materials discovery,” *Comput. Mat. Sci.* **58**, 218 (2012).
 - 31 “Icsd crystallographic database,” <https://icsd.fiz-karlsruhe.de/search/basic.xhtml>, accessed: Jan 2017.
 - 32 S. Zaima, Y. Shibata, H. Adachi, C. Oshima, S. Otani, A. Aono, and Y. Ishizawa, “Atomic chemical composition and reactivity of the TiC(111) surface,” *Surf. Sci* **157**, 380–392 (1985).
 - 33 A. Vojvodic, C. Ruberto, and B. I. Lundqvist, “Trends in atomic adsorption on titanium carbide and nitride,” *Surf. Sci.* **600**, 3619–3623 (2006).
 - 34 A. Zur and T. C. McGill, “Lattice match: An application to heteroepitaxy,” *J. Appl. Phys.* **55**, 378–386 (1984).
 - 35 R. O. Elliott and C. P. Kempter, “Thermal expansion of some transition metal carbides,” *J. Phys. Chem.* **62**, 630–631 (1958).
 - 36 L. G. Cota and P. de la Mora, “On the structure of lithium peroxide, Li₂O₂,” *Acta Cryst.* **B61**, 133–136 (2005).
 - 37 M. D. Radin, J. F. Rodriguez, F. Tian, and D. J. Siegel, “Lithium peroxide surfaces are metallic, while lithium oxide surfaces are not,” *J. Am. Chem. Soc.* **134**, 1093–1103 (2012).
 - 38 R. B. Araujo, S. Chakraborty, and R. Ahuja, “Unveiling the charge migration mechanism in Na₂O₂: Implications for sodium–air batteries,” *Phys. Chem. Chem. Phys.* **17**, 8203–8209 (2015).
 - 39 G. F. Carter and D. H. Templeton, “Polymorphism of sodium superoxide,” *J. Am. Chem. Soc.* **75**, 5247–5249 (1953).
 - 40 O. Arcelus, C. Li, T. Rojo, and J. Carrasco, “Electronic structure of sodium superoxide bulk, (100) surface, and clusters using hybrid density functional: Relevance for Na–O₂ batteries,” *Phys. Chem. Lett.* **6**, 2027–2031 (2015).
 - 41 K. C. Lau, R. S. Assary, P. Redfern, J. Greeley, and L. A. Curtiss, “Electronic structure of lithium peroxide clusters and relevance to lithiumair batteries,” *J. Phys. Chem. C* **116**, 23890 (2012).
 - 42 B. Hammer and J. K. Norskov, “Why gold is the noblest of all the metals,” *Nature* **376**, 238–240 (1995).
 - 43 J. K. Norskov, F. Abild-Pedersen, F. Studt, and T. Bligaard, “Density functional theory in surface chemistry and catalysis,” *PNAS* **108**, 937–943 (2011).
 - 44 T. Bligaard and J. K. Norskov, “Ligand effects in heterogeneous catalysis and electrochemistry,” *Electrochimica Acta* **52**, 5512–5516 (2007).
 - 45 C. Oshima, M. Aono, S. Zaima, Y. Shibata, and S. Kawai, “The surface properties of TiC(001) and TiC(111) surfaces,” *Journal of the Less-Common Metals* **82**, 69–74 (1981).